Articles

Physical Society of Indonesia

Journal of the Physical Society of Indonesia **1(2)**, 87-97 (2025)

https://doi.org/10.35895/jpsi.1.2.87-97.2025

Synthesis of rGO-TiO_2 Composite for Al-ion Battery with En-hanced Electrical Conductivity

Ruli Afian[1], Ferry Faizal[1,2], Camellia Panatarani[1,2], and I Made Joni[1,2*]

[1]*Department of Physics, Faculty of Mathematics and Natural Science, University of Padjadjaran, Sumedang, 45363, Indonesia*

[2]*Functional Nano Powder (FiNder) University Center of Excellence, University of Padjadjaran, Sumedang, 45363, Indonesia*

(Received August 01, 2025; revised October 06, 2025; accepted October 08, 2025; published online October 10, 2025)

Alternative batteries to lithium-ion are attracting growing attention due to the urgent demand for high energy density and limited lithium resources. Aluminum-ion (Al-ion) batteries are promising since aluminum is abundant, recyclable, and inexpensive. They also provide theoretically high specific energy and power through a three-electron redox reaction. However, challenges remain because no positive electrode material has yet shown efficient and reversible aluminum-ion storage. This study reports the synthesis of a reduced graphene oxide–titanium dioxide (rGO–TiO_2) composite and its evaluation as an electrode for Al-ion batteries. The rGO–TiO_2 composites were prepared by hydrothermal reaction with TiO_2 contents of 2, 5, and 10 wt.%. Characterization using X-ray diffraction (XRD), Raman spectroscopy, Fourier transform infrared spectroscopy (FTIR), and scanning electron microscopy (SEM) confirmed that graphite oxide (GO) was successfully reduced to rGO, as indicated by a peak at 2θ = 24.30°. Electrochemical testing of rGO–TiO_2 based Al-ion batteries showed improved ion diffusivity of $1.39 \times 10^{-6} - 3.83 \times 10^{-6}$ cm/s and charge–discharge capacities of 6.9–7.2 mAh/g at 1C (0.1–0.3 mA·g^{-1}). These results demonstrate the key role of enhanced ion diffusivity in advancing high-performance Al-ion batteries.

Keywords: *Aluminum-ion batteries, rGO–TiO_2 composite, Electrochemical performance, Ion diffusivity*

1. INTRODUCTION

The demand to meet net-zero carbon emissions goals needs a transition in the usage of renewable energy resources from the electric grid. This means that storing energy solutions will play a key role in mitigating climate change than ever before. A reliable stationary energy storage system is critical to the electrical grid, guaranteeing the power of renewable energy available, such as for buildings or for the integrated electric vehicle charging station. Therefore, the fastest-growing storage technology of batteries will play a key role in meeting every nation's goal of cutting greenhouse gas emissions. Creating affordable, sustainable, long-cycle life, and high-performance energy storage is therefore the next urgently needed and big challenge (Fazeli et al., 2019; Craig et al., 2020).

Batteries are currently being developed to power an increasingly diverse range of applications, large storage electrical grids, electric vehicles with extremely high specific energy batteries, etc. (Armand & Tarascon, 2008). Also, the challenge is to find alternative materials and designs that become more affordable to achieve widespread uptake of electric vehicles. Lithium-ion batteries currently dominate for new-build grid storage, electric vehicles, and electronic devices due to their outstanding specific energy and acceptable specific power. Moreover, the ever-growing demands for high-energy-density and ultrafast charging capability are triggering further improvements in rechargeable batteries (Hu et al., 2021). One of the most widely used materials today as electrodes is Lithium. However, the limited lithium resource (0.0065 wt% of the earth's crust) urges sustainable solutions (Yuan et al., 2020). Currently, both state-of-the-art and next-generation lithium-ion batteries have encountered bottlenecks in low energy density, poor durability, and severe safety issues, which might be difficult to overcome

*Contact Author: imadejoni@phys.unpad.ac.id

only by improving the performance of electrodes and electrolytes (Song et al., 2021). Aluminum-ion batteries are potential candidates for future large-scale energy storage devices owing to their advantages of high energy density, resource abundance, low cost, and environmental friendliness (Wu et al., 2021). The specific volumetric capacity of an Al anode is up to 8.046 mAh cm^3, close to 4 times higher compared with Li (2.062 mAh cm^3), with its gravimetric capacity (2.980 mAh/g) comparable to that of Li metal (3.860 mAh /g) (Yuan et al., 2020).

Despite the promising developments in aluminum-ion battery systems, challenges remain in optimizing cathode materials, particularly in achieving high reversibility and efficient ion transport (Zhang et al., 2018; Wang, 2014). Graphene is a material with a thickness of one atom composed of carbon atoms forming a hexagonal lattice (Setianto et al., 2023). Outperforming all other known cathode materials, graphene has made several remarkable breakthroughs in offering extraordinary energy density, power density, cycle life, thermal stability, safety, and flexibility (Minella et al., 2017; Das, 2018). In addition to graphene, another material that is widely used as an electrode material is titanium dioxide (TiO_2). TiO_2 arrays can ensure good electrode/electrolyte contact and serve as a fast diffusion pathway for electrolyte species due to the high surface area and unique nanosized geometry (Liu, 2012; Minella et al., 2017).

In practice, both graphene and TiO_2 as cathode materials have their advantages and disadvantages, but the disadvantages found in rGO can be overcome by combining them with TiO_2 in a hybrid or composite manner to improve electron transfer from the electrolyte (Low et al., 2019; Zhu et al., 2020; Zhang et al., 2018; Wang, 2014; Zafar et al., 2017; Lin et al., 2015; Vanitha et al., 2019; Tomasz et al., 2018; Rasheed et al., 2017). Therefore, this study aims to synthesize a reduced Graphene Oxide-Titanium Dioxide (rGO-TiO_2) composite and investigate its performance as an electrode for Aluminum-ion batteries.

2. METHOD

2.1 Materials

Graphene oxide (GO) was synthesized according to the modified Hummers method. The materials for GO synthesis by the modified Hummers method in this experiment were graphite (Merck), sodium nitrate ($NaNO_3$), sulfuric acid (H_2SO_4), potassium permanganate ($KMnO_4$), concentrated hydrochloric acid (HCl), and hydrogen peroxide (H_2O_2).

2.2 Synthesis of rGO-TiO_2

The preparation step is explained as follows: first, 2 g of graphite powder, 1 g of $NaNO_3$, and 45 mL of H_2SO_4 were stirred in an Erlenmeyer flask stored in an ice bath (0-5°C). The mixture was stirred for 30 minutes at 0-5°C, then 5 g of $KMnO_4$ was added to the suspension pinch by pinch. The addition of potassium permanganate is carefully controlled to keep the reaction temperature lower than 20°C. The mixture was stirred again for 30 minutes. Next, the ice bath was replaced with silicone oil. The mixture was stirred at 35°C for one hour in a silicon oil bath. After that, 45 ml of distilled water is slowly added to the mixture. The reaction temperature rapidly rose to 98°C, and the mixture was stirred for another 40 minutes. The mixture was diluted by adding 200 mL of distilled water and 25 mL of H_2O_2, then the mixture was stirred again for 30 minutes. For purification, the mixture was washed by adding 10 mL of HCl with deionized water and repeatedly washed using distilled water several times, and centrifuged for material separation. GO was dried in a drying oven and obtained in powder form. After that, the material is then converted into rGO by heating it in a microwave that is fed with argon/H_2.

$TiCl_3$ as much as 15% is mixed with aquades as much as 9 ml and concentrated HCl as much as 1.5 ml and then heated to 80°C with a hot plate temperature of 200°C. Next, concentrated HNO_3 is added and reheated to 80°C, then cleaned with ethanol and added aquades. The material is then dried at 100°C and then calcined at 200°C for 5 hours.

The synthesized rGO and TiO_2 are made composite materials by dissolving rGO with aquades and then sonicating for 3 hours. After that, the mixture is added to TiO_2 and then stirred for 3 hours. The solution of the material was transferred to the Teflon autoclave at 120°C for 15 hours. Next, the

temperature is lowered to room temperature, then the precipitate is washed using aquades to a normal pH. Furthermore, the material is put into a vacuum/oven at a temperature of 80 °C for 5 hours.

2.3 Characterization of rGO-TiO_2

XRD (PANalytical X'Pert HighScore), SEM (JSM-6360) were used to analyze the structure and morphologies of graphene. The Raman spectrum was measured by a laser Raman Spectrometer (LabRAM HR Evol). The surface morphology and lattice of rGO, TiO_2, and rGO-TiO_2 composites were observed by using Fourier Transform Infra-Red (FTIR Thermo Scientific Nicolet Is5 Thermo). The crystalline phases of the samples were determined via X-ray diffraction, XRD (D8 Advance X-ray diffractometer-Bruker AXS), by employing a Cu Kλ radiation source (1,54060 Å) at 40 kV and 30 mA with 0.02 deg/s.

2.4 Electrochemical Measurements

$AlCl_3$–[EMIm]Cl IL with a mole ratio of $AlCl_3$/[EMIm]Cl =1.3 was obtained. 1-ethyl-3-methylimidazolium chloride([EMIm]Cl 98%, Tokyo Chemical Industry Co., LTD) was dried under vacuum at 75 °C and 0.2 Torr for 16 h before use. $AlCl_3$ (99.99%, anhydrous powder, Lanhit) was commercially available and was used for the synthesis of ILs without additional preparation. The synthesis of ionic liquid was carried out in a UniLab MBraun glove box in a dry argon atmosphere (H_2O, $O_2 < 0.1$ ppm). Chloroaluminate IL was obtained by slowly adding $AlCl_3$ powder to [EMIm]Cl powder. As a result of mixing two solid salts at room temperature in certain proportions, a liquid with the required mole ratio of $AlCl_3$/[EMIm]Cl was obtained. IL synthesis was carried out immediately before electrochemical cell testing.

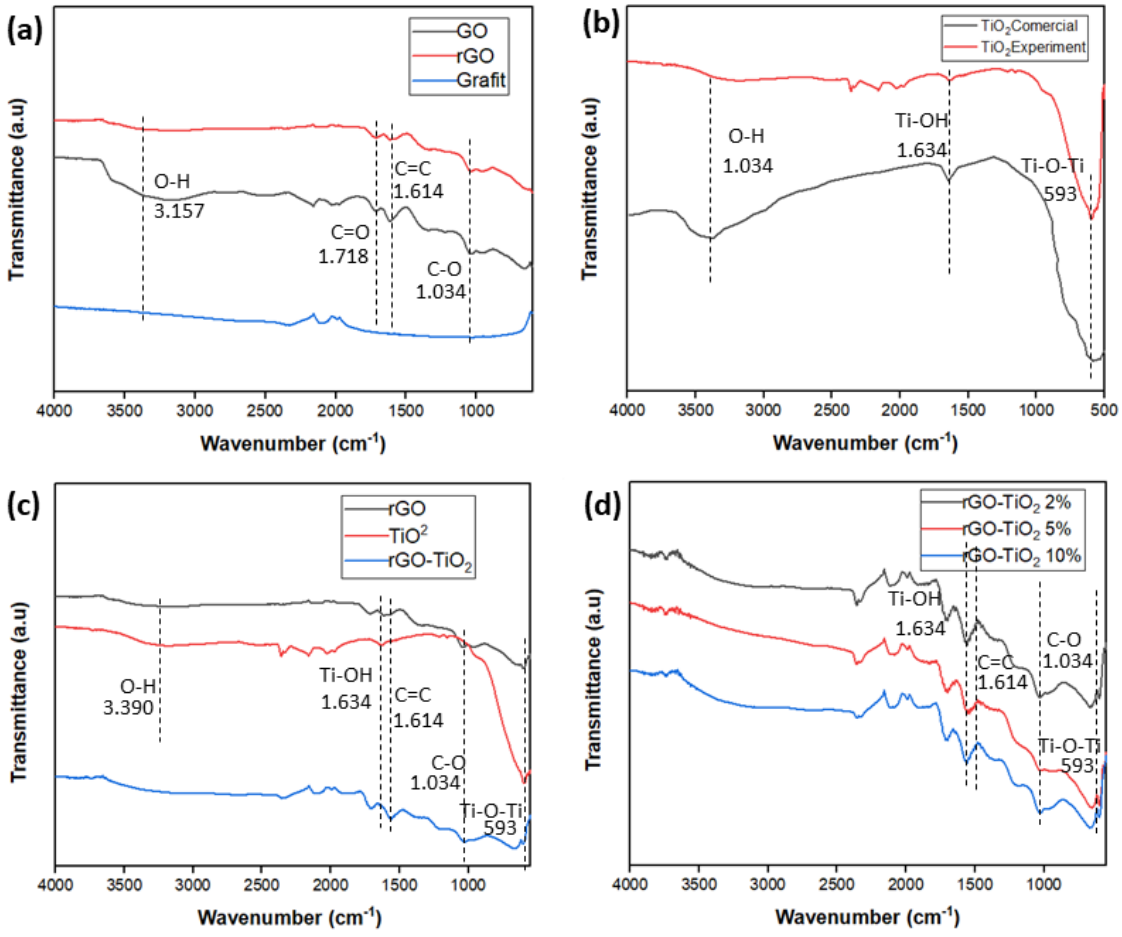

Figure 1. FTIR (a) Graphite GO, and rGO, (b) TiO_2, and (c) rGO, TiO2, and rGO-TiO2 (d) composite rGO-TiO2 with various TiO2 concentrations: 2wt%, 5wt%, and 10wt%.

The working electrode was fabricated from a well-dispersed slurry, which contained the active material (rGO-TiO_2), acetylene black, and polyvinylidene fluoride (PVDF) binder at the weight ratio of 80:10:10 in N-methyl-2-pyrrolidinone (NMP). After the above slurry was coated on Cu foils and dried in a vacuum oven at 110°C overnight. The cells used these active materials as the working electrode, and highly pure aluminum was used as the counter electrode and reference electrode. A CR2032 coin cell was used for evaluating electrochemical performances and was assembled in a glove box under an argon atmosphere. The galvanostatic charge-discharge was tested for a potential range of -0.1 to 0.1 V using the Land Battery Test System (Neware CT-ZWJ). Electrochemical impedance spectra (EIS) of rGO-TiO_2 for 50 cycles were tested at the electrochemical workstation (BST8-Stat).

3. RESULTS AND DISCUSSION

The characterization of functional groups is performed using the FTIR (Fourier Transform Infra-Red). The emerging molecular bonds are indicated by the presence of peaks in the FTIR chart pattern. Each molecular bond has a different wave number based on the ability of molecular bonds to vibrate and absorb energy from the infrared spectrum. In testing molecular bonds or functional groups, the sample is GO and rGO. Figure 1 shows the transmittance spectrum of the sample, and there are several functional group peaks. There are four peaks observed in the wavelength range of 4000–500 cm-1. The FTIR pattern qualitative in the GO sample showed that the main molecular bonds of the GO material were C = C, C-H, C-O, and C = O and O-H bonds. These bonds bind to each other to form a hexagonal structure of carbon atoms arranged into a GO layer. While the FTIR pattern qualitatively in the rGO sample showed that the main molecular bonds of the rGO material were in the form of C = C, C-H, and C-O bonds, and no O-H bonds were found, which means that oxygen has been reduced properly in the heating process using a microwave fed by argon/H_2 gas. The FTIR Spectrum of TiO_2 (Figure 1b) shows various characteristic peaks of TiO_2 experimental in comparison with the commercial TiO_2. Both spectra indicated the presence of Ti-OH, Ti-O-Ti, and O-H. Figure 1c shows the spectra of C=C, Ti-O-Ti, and Ti-OH bonds, indicating the formation of the rGO-TiO_2 composite. It was also found that the peak of the O-H bond was very low, indicating that O-H was reduced in both rGO and TiO_2. Figure 1d shows the spectra of rGO-TiO_2 at various TiO_2 concentrations, 2, 5, and 10 wt%. The results show that the same pattern of functional groups was observed.

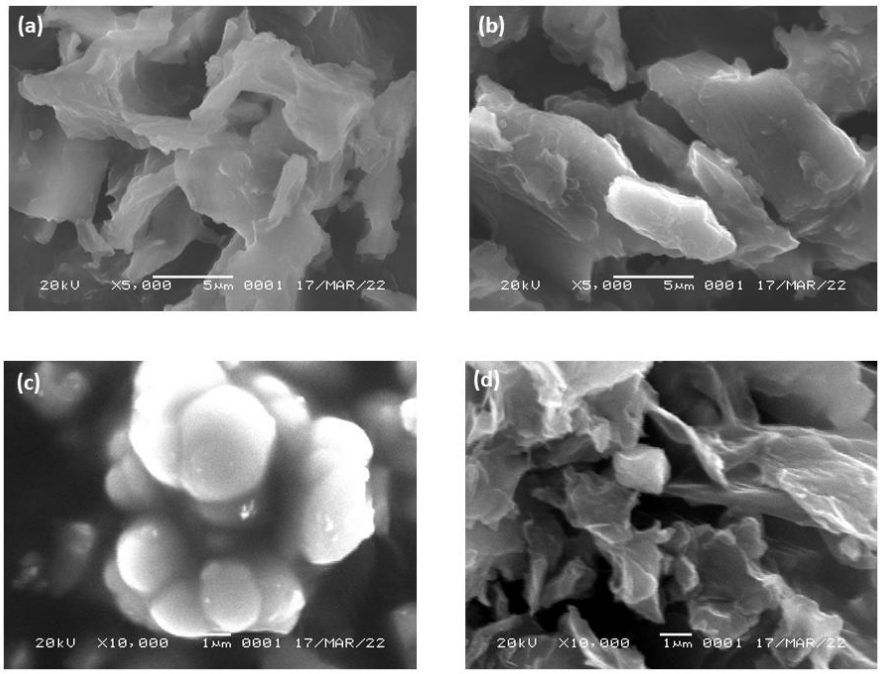

Figure 2. The SEM images of (a) GO, (b) rGO, (c) TiO_2, and (d) rGO-TiO_2

GO and rGO morphology was observed by SEM as shown in Figure 2a-b. The SEM images displayed the formation of the graphene sheet. These results indicated that graphite peeled off during the oxidation process. Also, an indication that graphene was a distorted sheet when oxygen and other functional groups are attached to the graphene sheet to form GO and rGO, and are evenly distributed with a wrinkled surface nature. This is due to the reduction of the functional group of oxygen in the GO due to the reduction process. In contrast, the SEM images of TiO_2 particles demonstrated spherical morphology with agglomeration occurring due to the aggregation of TiO_2 particles at high calcination temperatures, causing the acceleration of the growth of titanium dioxide crystals (Figure 2c). Moreover, the SEM image of rGO-TiO_2 composite shows that there were TiO_2 particles on the rGO surface, indicating that a composite was formed on the rGO sheet.

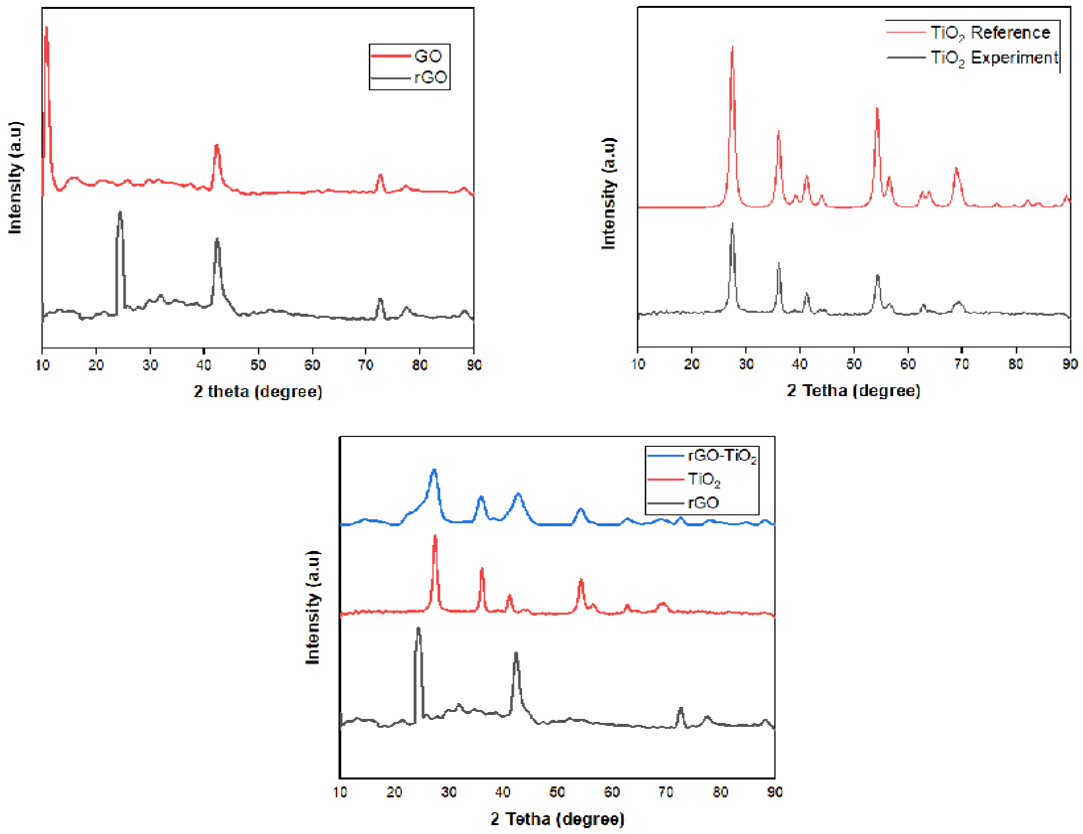

Figure 3. XRD Test Results on GO, rGO, TiO_2, and rGO-TiO_2

The XRD pattern on GO shows a peak of diffraction at $2\theta = 10.24°$ caused by graphite oxidation, which indicates that graphite has been fully oxidized to GO (Figure 3). A low-intensity diffraction peak at $2\theta = 42.10°$ indicates non-oxidized graphite. The XRD pattern on rGO indicates a shift in the peak of diffraction at $2\theta = 24.30°$ caused by the reduction of the oxygen group, which indicates that the rGO has formed. XRD pattern on TiO_2 In the sample, peaks corresponding to the rutile phase at an angle of 2 θ were observed at angles of 27.2°, 35.99°, 40.99°, 54.38°, 56.61°, 62.97°, 65.61°, and 86.63° when compared to references using match applications (Code [96-900-4143] TiO_2 Rutile) formed a pattern of peaks that tended to be the same. The peaks correspond to the crystal orientations at (004), (200), (105), (211), and (204). The XRD pattern on the rGO-TiO_2 composite shows peaks formed from a combination of peaks from rGO and TiO_2.

Raman spectroscopy provides information based on the inelastic scattering (Raman) of molecules irradiated by monochromatic light. Figure 4 shows the Raman spectrum of GO and rGO. The D vibration bands formed can be seen at 1344.86 cm^{-1} and 1348.80 cm^{-1} for GO and rGO. On the other hand, the vibration band G appears at 1597.65 cm^{-1} for GO and 1595.12 cm^{-1} for rGO. The vibrational band G also contributes to the presence of C-C bonding common in all carbon systems. The D band and

G band in the Raman spectrum symbolize the interference band and tangential band, respectively. Higher intensities in the D band also indicate that more isolated graphene is depicted in rGO compared to GO due to the loss of oxygen groups from GO after reduction.

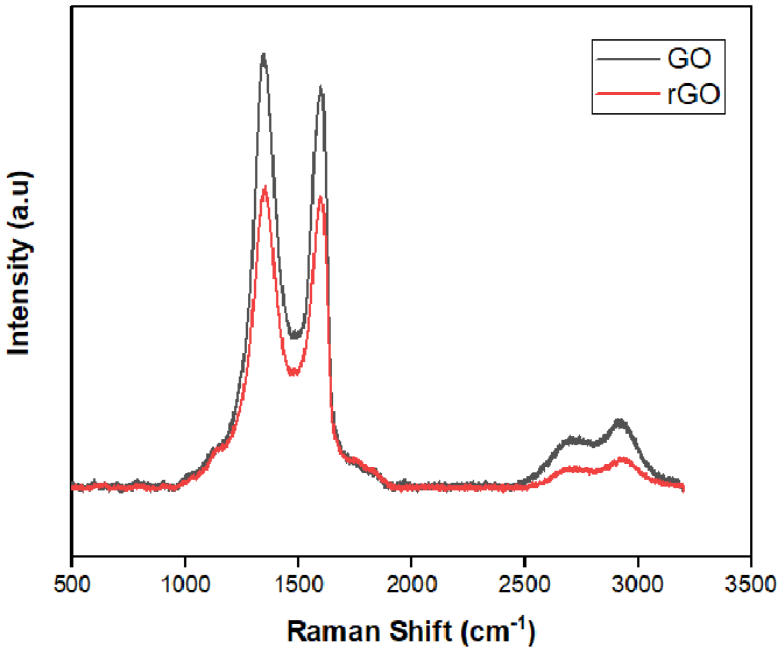

Figure 4. Raman Test Results on GO and rGO

The voltammogram graph of cyclic voltammetry measurement results in Aluminium-ion batteries with cathode composite rGO-TiO_2 variations of TiO_2 2wt%, 5wt%, and 10 wt% as shown in Figure 5. The result shows the difference in the amount of current generated during the charging and discharging process in each battery. During the charging process, there is a transfer where Aluminium ions move from the positive electrode (cathode) to the negative electrode (anode), called the oxidation peak. Otherwise, during the discharging process, there is a transfer process where Aluminium ions move from the negative electrode (anode) to the positive electrode (cathode), which is called the reduction peak. All three cathode variations exhibited oxidation peaks and reduction peaks. However, at variations of 2% and 5%, oxidation and reduction peaks were not very high compared to variations of 10%. Morphologically, the cathode in the 10% variation has a denser material compared to other variations, which causes the 10% variation to affect the transfer of electrons between particles. In addition, the surface area (surface area) affects the value of capacitance. In Cyclic Voltammetry, indicated by the curve, there are peaks of oxidation and reduction, in the voltage range of 0.6-0.8 V from each curve. The higher the concentration of TiO_2, the higher the peak of oxidation and reduction formed, so that the electric current produced was greater. High, sharp peaks indicate that the process of intercalation and deintercalation of aluminum ions is proceeding rapidly. From the data of the voltage and peak current of redox reactions, the magnitude of the diffusion coefficient of Al ions using the Randles-Sevcik equation (Wang, 2014):

$$i_p = 2.659 \times 10^5 n^{3/2} A C D^{1/2} v^{1/2} \quad (1)$$

where n is the number of electrons per molecule, surface area A (cm^2), C concentration of Al ions (mol/cm^3), D is the diffusion coefficient of Al ions, and v is the scanning rate (V/s), and i_p is the peak current (A). The results of the calculation of the diffusion coefficient can be seen in Table 1. The results show the difference in reduction and oxidation of each sample, indicated by the polarization voltage obtained from the distance between the reduction and oxidation peaks. In contrast, the diffusion coefficient of Al ions also increases with the addition of TiO_2 concentration, 3.834 $x10^{-6}$ for TiO_2 10 wt.% (Table 1). This diffusion is quite enhanced compared to another type of electrode found to be 2.806×10^{-14} (Wu et al., 2020).

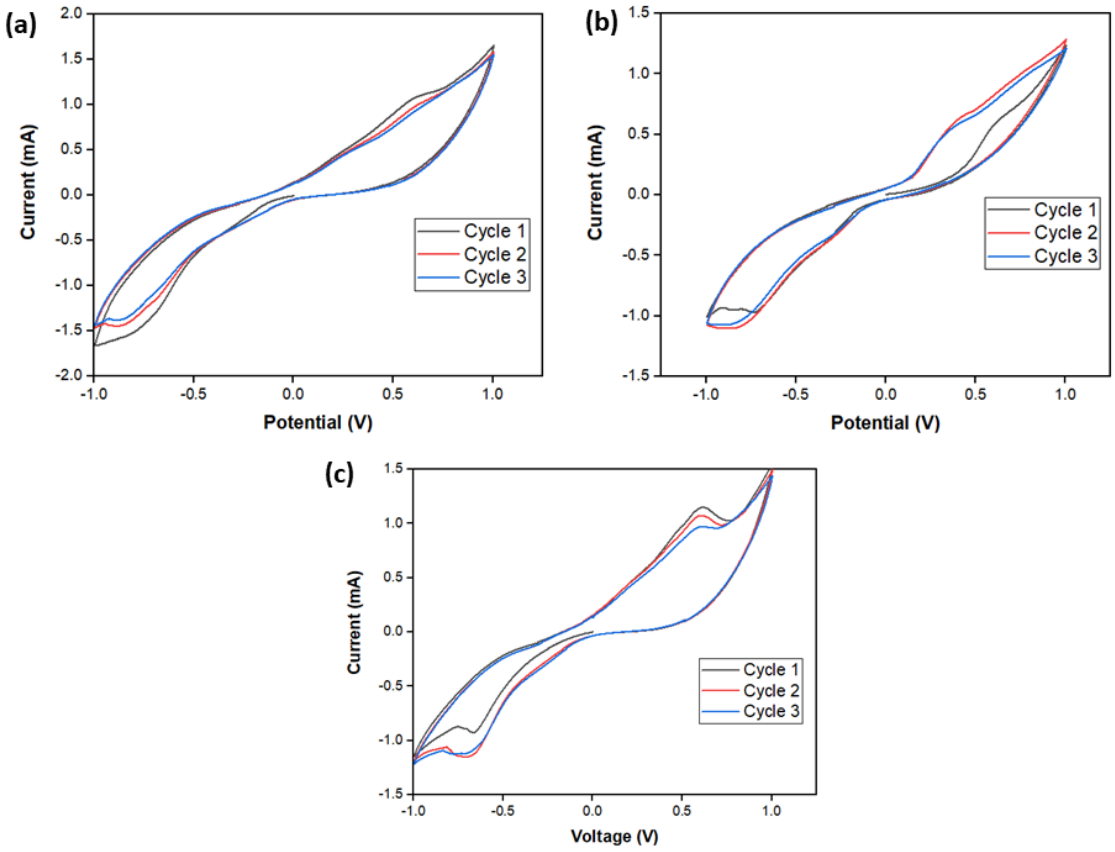

Figure 5. Cyclic Voltammetry of rGO-TiO_2 with variation of TiO_2: (a) 2wt%, (b) 5wt%, and (c) 10wt%

Table 1. Calculation of Al-ion diffusion coefficient

Varied TiO_2	Vred(volt)	Voks(volt)	Vpol(volt)	IPoks(mA)	P(mW)	D (cm/S)
2wt%	0.618	0.866	0.248	0.993	0.860	$3.339x10^{-6}$
5wt%	0.858	0.511	0.347	0.642	0.328	$1.390x10^{-6}$
10wt%	0.6937	0.6123	0.0813	1.0643	0.6517	$3.834 x10^{-6}$

Characterization with Electrochemical Impedance Spectroscopy (EIS) is carried out to determine the electrochemical properties, namely the impedance of the rGO-TiO_2 cathode and the conductivity value of the Al ions that intercalate during the charge/ discharge process. The impedance value obtained will determine the electrochemical properties of the cathode. The variation is carried out by adding the amount of TiO_2 in the rGO-TiO_2 composite by 2wt%, 5wt%, and 10wt% (Figure 6). After the sample was assembled into a battery in the form of a cell coin, the conductivity and impedance were obtained through Electrochemical Impedance Spectroscopy (EIS) testing at a frequency of 0.1 - 10000 Hz. This test is carried out by flowing AC in the battery so that the test results form an impedance that changes with the frequency function at a given AC. It is this impedance value that determines the electrochemical properties of the cathode, namely ionic collectivity (Li et. al., 2023, Qu et. al., 2022, Vadhva et al., 2021). The results of this test are represented in the Nyquist Plot. The value of the impedance is obtained to determine the intercalation process of aluminum ions that occurs between the interface at the rGO-TiO_2 cathode and the electrolyte solution. The shape of the EIS chart obtained was in the form of semicircles and slopes. The semicircle shows the process of transferring charges from aluminum ions on the surface of rGO-TiO_2 and the electrolyte. The Nyquist plot explains the relationship between real (Zreal) impedance and imaginary (Zimaginary) impedance at a given frequency, where the

real impedance is placed on the X-axis and the imaginary impedance on the Y-axis. The conductivity value can be calculated using the equation as follows (Shenouda & Liu, 2010):

$$R = \rho l/A \quad (2)$$

Where R is the resistance (Ω), the thickness of the sample, l (cm), the surface area of the sample, A (cm^2), and ρ is the resistivity. Conductivity ($\boldsymbol{\sigma}$) calculation data can be seen in Table 2. The diameter of a semicircle at high frequency can be attributed to the charge transfer resistance (Rct). R1 represents the resistance of the solution, reflecting the conductivity of the electrolyte, separator, and electrode (Shenouda & Liu 2010). EIS Test Results show rGO-TiO_2 Composites with TiO_2 variations of 2%, 5%, and 10% show different results. Only the 10% variation shows a semicircular pattern. This shows that the charge transfer of aluminum ions on the electrode surface and the electrolyte increases as more TiO_2 variations stick to the rGO surface. Therefore, it can be concluded that TiO_2 concentration helps increase the electrical conductivity of composites, making them more conductive and reversible.

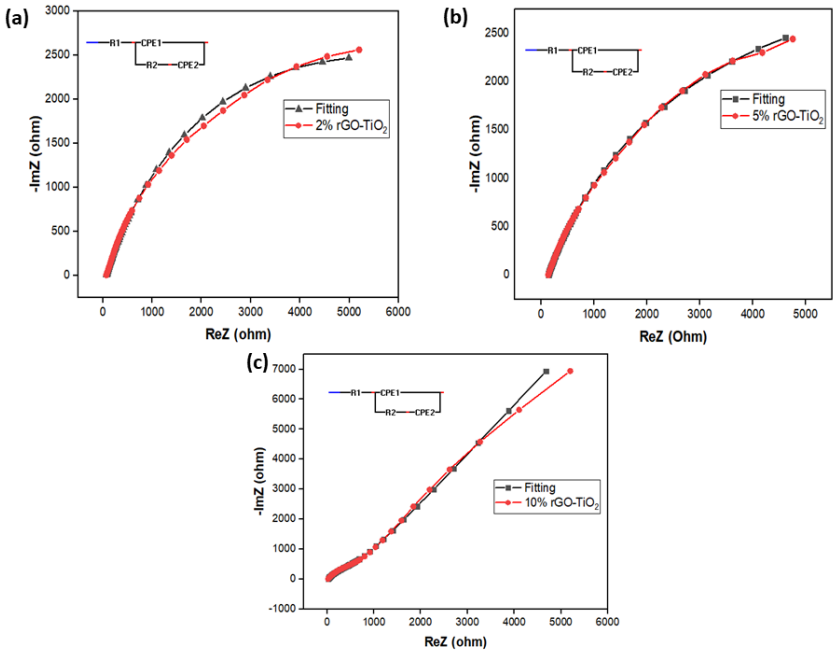

Figure 6. Electrochemical Impedance Spectroscopy (EIS) of rGO-TiO_2 with variation of TiO_2: (a) 2 wt%, (b) 5wt%, and (c) 10 wt%

Table 2. The conductivity of the cathode with variations of TiO_2

Varied TiO_2	Thickness (cm)	A (cm^2)	Re (**Ω**)	Rct (**Ω**)	$\boldsymbol{\sigma e(S/cm)}$	$\boldsymbol{\sigma ct}$(S/cm)	$\boldsymbol{\sigma}$ ((S/cm)
2 wt%	0.058	1.5386	69.521	5149.1	$12.836x10^{-4}$	$0.173x10^{-4}$	$13.009x10^{-4}$
5 wt%	0.073	1.5386	131.13	2.1477	$8.565x10^{-4}$	$522.967x10^{-4}$	$531.533x10^{-4}$
10 wt%	0.074	1.5386	18.049	1080.7	$63.081x10^{-4}$	$1.053x10^{-4}$	$64.135x10^{-4}$

Figure 7 shows the charge/discharge curve for the rGO-TiO_2 cathode in a coin cell aluminum ion battery with tests of 1 C with constant current at various TiO_2 concentrations: 2wt% at a current density of 0.178 mA/g, 5wt% at a current density of 0.275 mA/g, and 10wt% at a current density of 0.318 mA/g (Table 3). The charge-discharge test was conducted at 1 °C in each TiO2 variation for 50 cycles. The results show that the charged specific capacity was around 7 mAh /g, while the discharged specific capacity was lower, around 2 mAh /g. In contrast, the battery capacity increases as the TiO2

increases. However, in this preliminary study, the current density used in the test was quite high (1C); thus, reducing the C rate probably increases specific capacity, as also observed in other studies (Wu et. al., 2020). Since the cathode has very high diffusivity, it is meaningful to guide the direction of development for high-performance Al-ion batteries (Zhang et.al., 2020; Li et.al., 2021; Ashurov et. al., 2022; Yang et. al., 2022; Ma et al., 2023).

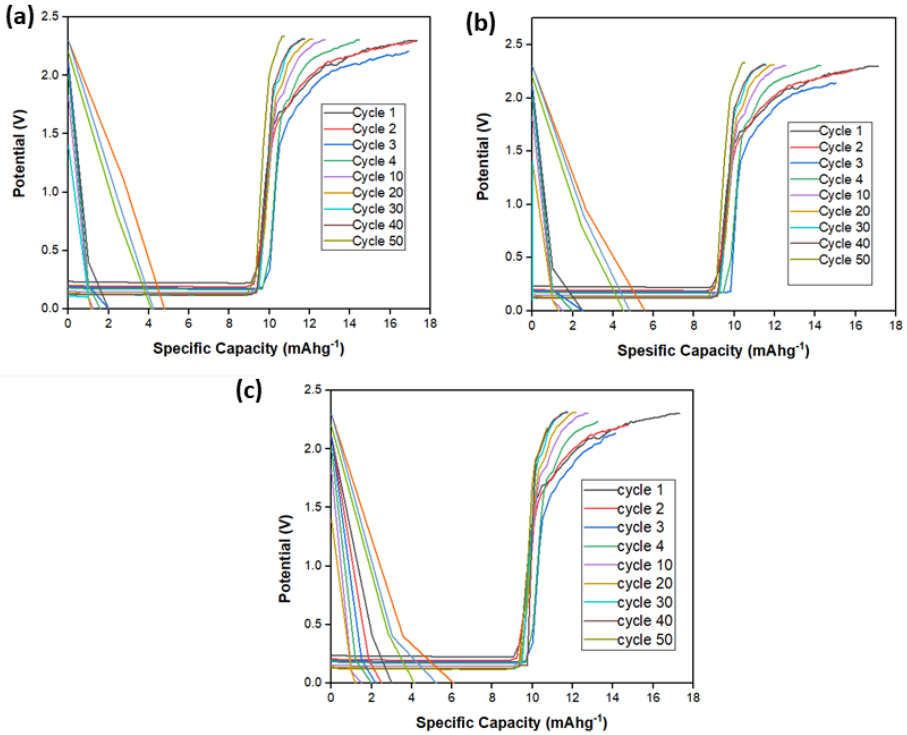

Figure 7. Charge discharge of rGO-TiO_2 with variation of TiO_2: (a) 2wt%, (b) 5wt%, and (c) 10wt%

Table 3. Charge-discharge analysis data 50 cycles with TiO_2 variations

TiO_2 Concentration	Specific Capacity		1 C Current Density* (mA/g)
	Charge (mAh/g)	Discharge (mAh/g)	
2 wt%	6.956	1.835	0.178
5 wt%	7.067	1.969	0.275
10 wt%	7.283	2.039	0.318

Note: * Calculation based on the theoretical capacity of rGO (298 mAh/g) and TiO_2 (4200 mAh/g).

4. CONCLUSION

The rGO-TiO_2 has been successfully synthesized and assembled into an aluminium ion battery coin cell with various TiO2 concentrations of 2, 5, and 10 wt%. The XRD and Raman spectra revealed that graphite oxide (GO) was successfully transformed to reduced graphene oxide (rGO). The electrochemical measurement of rGO-TiO2-based Al-Ion battery exhibited enhanced diffusivity 1.39 $\times 10^{-6}$-3.834$\times 10^{-6}$ cm/S and charge-discharge 6.9-7.2 mAh/g at 1 C (0.1-0.3 mA/g). It was concluded that the additional TiO_2 to the rGO-TiO_2 composite greatly influences the stability of electrons (electron transport) in aluminum-ion batteries, indicated by an increase in oxidation and reduction peaks at the concentration of TiO_2 10 wt%. Also, the density capacity at 10 wt% was greater than the other variations. Thus, the results are essential in guiding the development of high-performance Al-ion batteries with diverse current densities.

ACKNOWLEDGEMENT

The authors thank the financial support from the University of Padjadjaran under the schema of Academic Leadership Grant (ALG), contract number 1959/UN6.3.1/PT.00/2023.

REFERENCE

Armand, M., & Tarascon, J. M. (2008). Building better batteries. *Nature, 451(7179),* 652–657.

Ashurov, I., Iskandarov, S., Khalilov, U., & Ashurov, K. (2022). Current challenges, progress, and future perspectives of aluminum-ion batteries. *Applied Solar Energy, 58(3),* 334–354. https://doi.org/10.3103/S0003701X22030033.

Craig, B., Schoetz, T., Cruden, A., & de-Leon, C. P. (2020). Review of current progress in non-aqueous aluminium batteries. *Renewable and Sustainable Energy Reviews, 133,* 110100. https://doi.org/10.1016/j.rser.2020.110100.

Das, S. K. (2018). Graphene: A cathode material of choice for an aluminum-ion battery. *Angewandte Chemie International Edition. 57(51).* 16606-16617. https://doi.org/10.1002/anie.201802595.

Fazeli, M., Florez, J. P., & Simão, R. A. (2019). Improvement in adhesion of cellulose fibers to the thermoplastic starch matrix by plasma treatment modification. *Composites Part B: Engineering, 163,* 207–216.

Hu, Z., Liu, Q., Chou, S. L., & Dou, S. X. (2021). Two-dimensional material-based heterostructures for rechargeable batteries. *Cell Reports Physical Science, 2(1),* 100286.

Li, C., Hou, C. C., Chen, L., Kaskel, S., & Xu, Q. (2021). Rechargeable Al-ion batteries. *Energy Chemistry, 3*(2), 100049. https://doi.org/10.1016/j.enchem.2020.100049.

Li, Q., Yi, D., Dang, G., Zhao, H., Lu, T., Wang, Q., Lai, C., & Xie, J. (2023). Electrochemical impedance spectrum (EIS) variation of lithium-ion batteries due to resting times in the charging processes. *World Electric Vehicle Journal, 14(12),* 321. https://doi.org/10.3390/wevj14120321

Lin, M. C., Gong, M., Lu, B., Wu, Y., Wang, D. Y., Guan, M., Angell, M., Chen, C., Yang, J., Hwang, B. J., & Dai, H. (2015). An ultrafast rechargeable aluminum-ion battery. *Nature, 520(7547),* 324–328.

Liu, S., Hu, J. J., Yan, N. F., Pan, G. L., Li, G. R., & Gao, X. P. (2012). Aluminum storage behavior of anatase TiO_2 nanotube arrays in aqueous solution for aluminum ion batteries. *Energy & Environmental Science, 5*(12), 9743.

Low, F. W., Lai, C. W., Asim, N., Akhtaruzzaman, M., Alghoul, M., Tiong, S. K., & Amin, N. (2019). An investigation on titanium doping in reduced graphene oxide by RF magnetron sputtering for dye-sensitized solar cells. *Solar Energy, 188,* 10–18.

Ma, D., Yuan, D., de-León, C. P., Jiang, Z., Xia, X., & Pan, J. (2023). Current progress and future perspectives of electrolytes for rechargeable aluminum-ion batteries. *Energy & Environmental Materials, 6(1),* e12301. https://doi.org/10.1002/eem2.12301.

Minella, M., Versaci, D., Casino, S., Di Lupo, F., Minero, C., Battiato, A., Penazzi, N., & Bodoardo, S. (2017). Anodic materials for lithium-ion batteries: TiO_2-rGO composites for high power applications. *Electrochimica Acta, 230,* 132–140. https://doi.org/10.1016/j.electacta.2017.01.190.

Qu, D., Ji, W., & Qu, H. (2022). Probing process kinetics in batteries with electrochemical impedance spectroscopy. *Communications Materials, 3(1),* 61. https://doi.org/10.1038/s43246-022-00284-w.

Rasheed, R. T., Al-Algawi, S. D., & Rhoomi, Z. R. (2017). Synthesis and antibacterial activity of rutile-TiO_2 nanopowder prepared by hydrothermal process. *Pure and Applied Sciences, 25(5),* 1744–1754.

Setianto, S., Panatarani, C., Singh, D., & Joni, I. M. (2023). Semi-empirical infrared spectra simulation of pyrene-like molecules: Insight for simple analysis of functionalization graphene quantum dots. *Scientific Reports, 13(1),* 2282. https://doi.org/10.1038/s41598-023-29486-z.

Shenouda, A. Y., & Liu, H. K. (2010). Preparation, characterization, and electrochemical performance of Li_2CuSnO_4 and $Li_2CuSnSiO_6$ electrodes for lithium batteries. *Journal of the Electrochemical Society, 157(11),* A1183. https://doi.org/10.1149/1.3479425

Song, Y., Sheng, L., Wang, L., Xu, H., & He, X. (2021). From separator to membrane: Separators can function more in lithium-ion batteries. *Electrochemistry Communications, 124,* 106948.

Tomasz, K., Wojciech, J. K., & Jagoda, L. (2018). Biomedical applications of graphene-based structures. *Nanomaterials, 8(11),* 944.

Vadhva, P., Hu, J., Johnson, M. J., Stocker, R., Braglia, M., Brett, D. J. L., & Rettie, A. J. E. (2021). Electrochemical impedance spectroscopy for all-solid-state batteries: Theory, methods and future outlook. *ChemElectroChem, 8(11),* 1930–1947.

Vanitha, M., Joni, I. M., Wibawa, B. M., & Panatarani, C. (2019). Metal oxides, metal sulphides and hybrid cathode materials for aluminium ion batteries – A mini review. *IOP Conference Series: Materials Science and Engineering, 550(1),* 012003.

Wang, J. (2014). *Analytical electrochemistry* (2nd ed., pp. 100–140). Wiley-VCH.

Wu, J., Wu, D., Zhao, M., Wen, Z., Jiang, J., Zeng, J., & Zhao, J. (2020). Rod-shaped $Cu_{1.81}Te$ as a novel cathode material for aluminum-ion batteries. *Dalton Transactions, 49(3),* 729–736.

Wu, X., Qin, N., Wang, F., Li, Z., Qin, J., Huang, G., & Deng, J. (2021). Reversible aluminum ion storage mechanism in Ti-deficient rutile titanium dioxide anode for aqueous aluminum-ion batteries. *Energy Storage Materials, 37,* 619–627.

Yang, Z., Wang, F., Meng, P., Luo, J., & Fu, C. (2022). Recent advances in developing organic positive electrode materials for rechargeable aluminum-ion batteries. *Energy Storage Materials, 51,* 63–79. https://doi.org/10.1016/j.ensm.2022.06.018

Yuan, D., Zhao, J., Manalastas, W. J., Kumar, S., & Srinivasan, M. (2020). Emerging rechargeable aqueous aluminum ion battery: Status, challenges, and outlooks. *Nano Materials Science, 2(3),* 248–263.

Zafar, Z. A., Imtiaz, S., Razaq, R., Ji, S., Huang, T., Zhang, Z., Huang, Y., & Anderson, J. A. (2017). Cathode materials for rechargeable aluminum batteries: Current status and progress. *Journal of Materials Chemistry A, 5(12),* 5646–5660.

Zhang, K., Kirlikovali, K. O., Suh, J. M., Farha, O. K., Choi, J. W., Jang, H. W., Varma, R. S., & Shokouhimehr, M. (2020). Recent advances in rechargeable aluminum-ion batteries and considerations for their future progress. *ACS Applied Energy Materials, 3*(7), 6019–6035.

Zhang, Y., Liu, S., Ji, Y., Ma, J., & Yu, H. (2018). Emerging nonaqueous aluminum-ion batteries: Challenges, status, and perspectives. *Advanced Materials, 30*(38), 1706310. https://doi.org/10.1002/adma.201706310

Zhu, N., Wu, F., Wang, Z., Ling, L., Yang, H., Gao, Y., Guo, S., Suo, L., Li, H., Xu, H., Bai, Y., & Wu, C. (2020). Reversible Al^{3+} storage mechanism in anatase TiO_2 cathode material for ionic liquid electrolyte-based aluminum-ion batteries. *Journal of Energy Chemistry, 51,* 72–80. https://doi.org/10.1016/j.jechem.2020.03.032